

1 **Two contrasting views of multidecadal climate variability in the 20<sup>th</sup> century**

2 Sergey Kravtsov<sup>1\*</sup>, Marcia G. Wyatt<sup>2</sup>, Judith A. Curry<sup>3</sup>, and Anastasios A. Tsonis<sup>1</sup>

3

4 **Keywords:** global warming, forced vs. intrinsic climate variability, stadium wave

5 **Index Terms:** 0550, 1616, 1620, 1626, 3305

6

7 **Key points:**

- 8 • An objective filtering method identifies a global mode of climate variability
- 9 • Space–time structure of climate in historic simulations reflects forced signal
- 10 • Modeled multidecadal climate variations are too weak, especially in atmosphere

11

---

<sup>1</sup> Department of Mathematical Sciences, Atmospheric Science group, University of Wisconsin-Milwaukee, P. O. Box 413, Milwaukee, WI 53201

\* Corresponding author email: [kravtsov@uwm.edu](mailto:kravtsov@uwm.edu)

<sup>2</sup> Department of Geological Sciences, University of Colorado, Boulder, CO

<sup>3</sup> School of Earth and Atmospheric Sciences, Georgia Institute of Technology, Atlanta, GA

1

2 **Abstract:** The bulk of our knowledge about causes of 20<sup>th</sup> century climate change comes  
3 from simulations using numerical models. In particular, these models seemingly  
4 reproduce the observed nonuniform global warming, with periods of faster warming in  
5 1910–1940 and 1970–2000, and a pause in between. However, closer inspection reveals  
6 some differences between the observations and model simulations. Here we show that  
7 observed multidecadal variations of surface climate exhibited a coherent global-scale  
8 signal characterized by a pair of patterns, one of which evolved in sync with multidecadal  
9 swings of the global temperature, and the other in quadrature with them. In contrast,  
10 model simulations are dominated by the stationary — single pattern — forced signal  
11 somewhat reminiscent of the observed “in-sync” pattern most pronounced in the Pacific.  
12 While simulating well the amplitude of the largest-scale — Pacific and hemispheric —  
13 multidecadal variability in surface temperature, the model underestimates variability in  
14 the North Atlantic and atmospheric indices.

## 15 **1. Introduction**

16 Multidecadal variations in the rate of global warming over the course of 20<sup>th</sup> century  
17 may reflect a combination of nonlinear changes in external forcing [*Nagashima et al.*,  
18 2006; *Meehl et al.*, 2007; *Booth et al.*, 2012; *Evan*, 2012] with a global expression of  
19 intrinsic climate variability superimposed on forced warming trends [*Folland et al.*, 1984;  
20 *Ghil and Vautard*, 1991; *Schlesinger and Ramankutti*, 1994; *Delworth and Mann*, 2000].  
21 Relative contributions from the forced and intrinsic components are still being debated.  
22 In particular, evidence from climate models implies a limited role for intrinsic variability  
23 [*Knight et al.*, 2005; *Delworth et al.*, 2007; *Booth et al.*, 2012; *Evan*, 2012]. On the other

1 hand, observational studies indicate a more ubiquitous hemispheric signature of  
2 multidecadal climate variations, implying a more complex climate evolution [*Minobe*,  
3 1997, 1999; *Enfield et al.*, 2001; *Wyatt et al.*, 2012].

4 Coupled models do produce synthetic climates that exhibit intrinsic (unforced)  
5 multidecadal variability in the North Atlantic region. However, the hemispheric and  
6 global expressions of this variability were generally too weak to rationalize the observed  
7 nonuniformity of the global warming rate [*Knight et al.*, 2005; *Delworth et al.*, 2007]. A  
8 natural conclusion was that other factors must have contributed to the 20–30-yr-long mid-  
9 century pause in global warming, with the most likely candidate being a forced climate  
10 cooling by the tropospheric aerosols [*Nagashima et al.*, 2006]. Some recent studies  
11 suggested that aerosol forcing dominates multidecadal climate signal in the 20<sup>th</sup> century  
12 not only globally, but also regionally over the North Atlantic Ocean [*Booth et al.*, 2012;  
13 *Evan*, 2012], while others emphasized large uncertainties associated with both natural  
14 and anthropogenic aerosol forcing on climate [*Carshaw et al.*, 2012; *Stevens*, 2013].

15 Following *Tsonis et al.* [2007], *Wyatt et al.* [2012] considered a network of climate  
16 indices associated, geographically and dynamically, with different climatic subsystems,  
17 and used an objective filtering method to isolate secular multidecadal variability within  
18 this network during the 20<sup>th</sup> century. On top of a uniform linear trend, they identified an  
19 oscillatory-looking wiggle with a common multidecadal time scale, but with different  
20 phases across the different indices of the climate network, thus manifesting a signal that  
21 propagates in the space of climate indices. The authors termed this propagating signal the  
22 “stadium wave,” reflecting a speculation that it dynamically originates in the North  
23 Atlantic and spreads over the remainder of the Northern Hemisphere via a hypothesized

1 sequence of delayed dynamical feedbacks. However, search for the stadium wave in a  
2 suite of simulations by multiple global climate models only returned stationary, in-phase  
3 signals [*Wyatt and Peters, 2012*], in sharp contrast with the observational analysis of  
4 *Wyatt et al. [2012]*.

5 There are two possible explanations for this documented inconsistency between  
6 climate model simulations and observations. The first one is that the propagation detected  
7 by *Wyatt et al. [2012]* is an artifact of their statistical analysis and the lagged phasing of  
8 various climate indices is entirely due to sampling [*Mann et al., 2014*]. An alternative  
9 explanation is that a coherent propagating multidecadal climate signal in the Northern  
10 Hemisphere is real, in which case one needs to look further into the inability of climate  
11 models to simulate this signal. The goals of this letter are to: (i) establish robustness of  
12 the observed 20<sup>th</sup>-century stadium-wave signal and refute the Mann et al. (2014)  
13 conjecture; and (ii) document and analyze the differences between the observed secular  
14 climate variability and the one simulated by a state-of-the-art climate model.

15

## 16 **2. Data and methods**

### 17 **2.1 Data sources**

18 We analyzed two-dimensional global monthly sea-surface temperature (SST) and  
19 sea-level pressure (SLP) time series based on the Extended Reconstructed Sea-Surface  
20 Temperature (ERSST.v3b) data set [*Smith et al., 2008*] and the 20<sup>th</sup> century reanalysis  
21 (NCEP-20) data set [*Compo et al., 2011*]. In addition, we considered five available  
22 historical 20<sup>th</sup> century simulations by Geophysical Fluid Dynamics Laboratory Coupled

1 Physical Model, CM3 [Donner *et al.*, 2011], hereafter GFDL CM3. For each of these  
2 data sets, we computed their associated climate index networks. We also used an original  
3 network of climate indices from Wyatt *et al.* [2012], which is based on alternative data  
4 sources (see **Table 1**).

5

## 6 **2.2 Methodology**

7 Following Wyatt *et al.* [2012], we defined the 20<sup>th</sup>-century secular climate variability  
8 in the climate-index networks considered as the sum of a linear trend and a dominant  
9 multidecadal signal. This signal was objectively identified via multi-channel version of  
10 the Singular Spectrum Analysis [SSA: Broomhead and King, 1986; Elsner and Tsonis,  
11 1996] called M-SSA [Moron *et al.*, 1998; Ghil *et al.*, 2002]. M-SSA is an extended  
12 variant of a widely used Empirical Orthogonal Function (EOF) analysis technique  
13 [Monahan *et al.*, 2009], which looks for the space–time patterns that maximize lagged  
14 covariance for a given multivariate time series within a range of  $M$  lags. The original raw  
15 time series can be fully recovered as the sum, over all modes, of the so-called  
16 reconstructed components (RCs) associated with each M-SSA mode. The secular  
17 multidecadal signal for the time series considered here is well represented by the sum of  
18 two leading RCs, which we will hereafter refer to as the stadium-wave signal. While the  
19 secular variability has, by definition, timescales exceeding the M-SSA window  $M$ , the M-  
20 SSA can identify time delays of up to  $M$  time units between different indices (channels)  
21 comprising the climate network. In the analysis below, we used annual data and  $M=30$ .

1 Note that our method for decomposing the climate variability into linear trend,  
2 multidecadal stadium-wave signal and the residual components is purely statistical and  
3 cannot be used for signal attribution. It is likely, however, that the trend is forced and the  
4 residual variability — which is predominantly interannual — is intrinsic, while the  
5 stadium wave may be a combination of the intrinsic and forced signals.

6

### 7 **3. Results**

#### 8 **3.1 Observed multidecadal climate variability in the 20<sup>th</sup> century**

9 The stadium wave (**Fig. 1**, left panel) for the set of annual indices in Table 1  
10 exhibits a common multidecadal signal, with widespread phase shifts between the  
11 individual-index RCs defining a striking propagation across the space of climate indices  
12 emphasized by *Wyatt et al.* [2012]. *Mann et al.* [2014] correctly pointed out that the  
13 phases of the stadium-wave components are subject to uncertainty. We devised the  
14 following Monte-Carlo procedure to estimate this uncertainty. This procedure is  
15 analogous in spirit to the one used by Mann et al. (2014) to demonstrate artificial  
16 propagation in a synthetic climate network, but does not require the *a priori* knowledge  
17 of the forced signal. Upon computing the decomposition of our climate-index network  
18 into the linear trend, multidecadal secular signal and the residual time series, we  
19 produced surrogate realizations of the residual using a linear stochastic model constructed  
20 to statistically reproduce the observed residual's lag-0 and lag-1 covariance structure.  
21 Adding the surrogate residual time series to the actual linear trend and stadium-wave  
22 signal resulted in surrogate versions of the original climate network. These surrogate

1 networks were then subjected to the same decomposition procedure as the original  
2 network: that is, subtraction of a new linear trend, and identification of a new leading M-  
3 SSA based stadium-wave signal, which can indeed be phase shifted with respect to the  
4 original signal due to sampling variations (see Fig. 1, right panel). However, repeating  
5 surrogate stadium wave identification 1000 times to compute phase uncertainties  
6 demonstrated that these variations are insufficient to explain the observed phase spread  
7 among individual stadium-wave components (**Table 2**), thus suggesting that the observed  
8 stadium-wave propagation is real. Our procedure thus presents evidence to refute the  
9 Mann et al. (2014) conjecture about artificial propagation of the observed stadium wave.  
10 The same results were obtained for the climate index network based on an alternative  
11 ERSST/NCEP-20 data set (see Supporting Information).

12

### 13 **3.2 Multidecadal climate variability in the GFDL CM3 model's 20<sup>th</sup> century** 14 **runs**

15 Unlike the observed stadium wave, the stadium waves identified in the *individual*  
16 GFDL CM3 20<sup>th</sup> century simulations exhibit a common shape which is characterized by  
17 in-phase signal dominated by the SST-based indices (see Supporting Information). The  
18 ensemble-mean over these five individual “stadium waves” is shown in the left panel of  
19 **Fig. 2**. The common shape and phasing of these individual “stadium waves” across  
20 different realizations of the GFDL CM3 simulated 20<sup>th</sup> century climate indicates that this  
21 signal describes the forced climate response. This forced signal in fact dominates the *total*  
22 multidecadal variability in the GFDL model, while the residual intrinsic variability in the

1 individual GFDL runs has interannual-to-decadal timescales (not shown). The in-phase,  
2 stationary character of the forced stadium wave in the GFDL model means that it can be  
3 well described by a single time series, which we objectively computed as the leading  
4 EOF of the set of stadium-wave reconstructions for each individual GFDL run. Indeed,  
5 such EOFs account for a major fraction of the reconstructed variance in each run, and  
6 well approximate the shape of the forced signal (Fig. 2, right panel).

### 7 **3.3 Patterns, magnitudes and time scales of hemispheric teleconnections**

8 The results of the above analysis show that the observed and simulated  
9 multidecadal climate variations are fundamentally different: the observations involve  
10 contributions from at least two spatial patterns to rationalize the stadium-wave  
11 propagation, while the model simulations can be well described by the stationary stadium  
12 wave characterized by a single pattern. We defined these patterns by regressing the  
13 observed and simulated SST fields onto the normalized sine and cosine predictors, with  
14 the period of 75 yr and the zero phase at year 1920. The sine predictor is thus aligned  
15 with the multidecadal undulations of the global temperature time series, in particular,  
16 with its downswing between 1940 and 1970. It also roughly corresponds to the shape of  
17 the GFDL CM3's "stadium wave" (Fig. 2). While the GFDL CM3 based linear trend and  
18 sine patterns are reasonably consistent with their observational analogues, the cosine  
19 pattern, which is quite pronounced in observations, is essentially absent from model  
20 simulations (**Fig. 3**), indeed in line with our earlier stadium-wave diagnosis (see  
21 Supporting Information for SLP analysis and animations of the observed and simulated  
22 multidecadal variability).

1           Note that the simulated patterns shown in Fig. 3 are based on the ensemble  
2 averages of the GFDL CM3 20<sup>th</sup> century runs. This is justified by the fact that the  
3 simulated secular forced signal (trend + multidecadal stadium wave) — which is  
4 essentially the same in all of the individual GFDL runs — completely dominates the  
5 secular variability in these runs, whereas the residual intrinsic variability in all model  
6 simulations has interannual-to-decadal time scales at most (not shown). Thus, the  
7 intrinsic *multidecadal* variability doesn't contribute much to the GFDL CM3's dominant  
8 stadium wave (see Fig. 2).

9           Furthermore, comparing the spectra of the observed and simulated climate-  
10 network indices (**Fig. 4**) shows that the *total* variance levels of the secular climate  
11 variability in observations and models are also very different for some of the indices  
12 considered. We must note first that the GFDL model does a very good job in reproducing  
13 observed variances of the indices representing secular climate signal on the largest spatial  
14 scale, namely, the PDO and NHT indices and, by this measure, provides a skillful  
15 simulation of the observed large-scale climate variability. This suggests that the  
16 combination of forced and intrinsic decadal variability of Pacific SSTs dominates the  
17 NHT's decadal variability, consistent with the results of *Kosaka and Xie* [2013].  
18 However, while the variances of all raw climate indices are comparable between the  
19 observed and GFDL CM3 based climate networks, the simulated atmospheric indices, as  
20 well as the SST indices representing the relatively smaller but important Atlantic sector,  
21 namely the AMO and DP indices, have variances in the decadal-to-multidecadal range  
22 that are strikingly smaller than the observed variances by up to an order of magnitude. In  
23 summary, the bulk of the evidence suggests that the GFDL CM3's simulated leading

1 multidecadal variations in the 20<sup>th</sup> century are due to the forced signal dominated by the  
2 Pacific sector and synchronized with the Northern Hemisphere's temperatures, while the  
3 multidecadal variance in the Atlantic SSTs and the atmosphere is much weaker than the  
4 observed variance.

5

#### 6 **4. Summary and discussion**

7 Our analysis demonstrates that, within the constraints imposed by a limited  
8 observational record, the spatiotemporal structure of multidecadal variability in the  
9 GFDL CM3 model exhibits noticeable differences from the observed 20<sup>th</sup>-century climate.  
10 In particular, while capturing the secular signal in the Pacific and hemispherically  
11 averaged surface temperatures very well, the simulated climate fails to exhibit  
12 multidecadal atmospheric (SLP) variations comparable in magnitude with the observed  
13 SLP variations; the simulated multidecadal SST variability in the Atlantic sector is also  
14 underestimated. Furthermore, the model is missing the lagged spatial coherence between  
15 different regional climatic fields characteristic of the observed multidecadal climate  
16 variability. Consequently, irrespective of the cause of the observed variability — natural,  
17 forced or combined — there could be some physical processes, probably operating in the  
18 Atlantic sector of the climate system, that are not well represented in the GFDL model.  
19 Possible candidates include lack of atmospheric sensitivity to ocean induced SST  
20 anomalies [*Kushnir et al.*, 2002], inaccurate parameterization of the mesoscale ocean  
21 eddies [*Kravtsov et al.*, 2011], or distortion of sea-ice effects on the high-latitude air–sea

1 interaction [*Wyatt and Curry*, 2014]. Examining these issues is a worthwhile subject for  
2 future studies.

3 **Acknowledgements.** All data and MATLAB © scripts for this paper are available for  
4 downloading from <http://pantherfile.uwm.edu/kravtsov/www/KWCT2014> (see  
5 Supporting Information for details). We are grateful to four anonymous reviewers for  
6 their comments, which helped to clarify and balance the presentation. This research was  
7 supported by the NSF grants OCE-1243158 (SK), AGS-1408897 (SK and AAT), as well  
8 as by the 2013 University of Wisconsin-Milwaukee Research Growth Initiative grant  
9 101X286 and DOE grant DE-SC0005305 (AAT).

1 **References**

- 2 Beamish R. J., et al. (1997), Production of Fraser River sockeye salmon (*Oncorhynchus*  
3 *nerka*) in relation to decadal-scale changes in the climate and the ocean, *Can. J.*  
4 *Fish. Aquat. Sci.*, 54, 543–554, 10.1139/f96-310.
- 5 Booth, B. B. B., et al. (2012), Aerosols implicated as a prime driver of twentieth-century  
6 North Atlantic climate variability, *Nature*, 484, 228–232,  
7 doi:10.1038/nature10946.
- 8 Broomhead D. S., and G. P. King (1986), Extracting qualitative dynamics from  
9 experimental data, *Phys. D*, 20, 217–236, <http://dx.doi.org/10.1016/0167->  
10 [2789\(86\)90031-X](http://dx.doi.org/10.1016/0167-2789(86)90031-X).
- 11 Brohan, P., et al. (2006), Uncertainty estimates in regional and global observed  
12 temperature changes: a new dataset from 1850, *J. Geophys. Res.*, 111, D12106,  
13 doi:10.1029/2005JD006548.
- 14 Carslaw, K. S., et al. (2013), Large contribution of natural aerosols to uncertainty in  
15 indirect forcing, *Nature*, 503, 67–71, doi:10.1038/nature12674.
- 16 Compo, G. P., et al. (2011), The twentieth century reanalysis project, *Quart. J. Royal*  
17 *Meteor. Soc.*, 654, 1–28, doi: 10.1002/qj.776.
- 18 Delworth, T. L., and M. E. Mann (2000), Observed and simulated multidecadal  
19 variability in the Northern Hemisphere, *Climate Dyn.*, 16, 661–676, doi:  
20 10.1007/s003820000075.
- 21 Delworth, T. L., et al. (2007), Decadal to Centennial Variability of the Atlantic from  
22 Observations and Models, in *Past and Future Changes of the Oceans Meridional*  
23 *Overturning Circulation: Mechanisms and Impacts*, *Geophys. Monogr. Ser.*, vol.

1 173, edited by A. Schmittner, J. C. H. Chiang, and S. R. Hemming, pp.131–148,  
2 AGU, Washington, D. C.

3 Donner, L. J., et al. (2011), The dynamical core, physical parameterizations, and basic  
4 simulation characteristics of the atmospheric component AM3 of the GFDL  
5 global coupled model CM3, *J. Climate*, 24, 3484–3519, doi:  
6 <http://dx.doi.org/10.1175/2011JCLI3955.1>.

7 Elsner, J. B., and A. A. Tsonis (1996), *Singular spectrum analysis: A new tool in time*  
8 *series analysis*, Springer, New York.

9 Enfield, D. B., et al. (2001), The Atlantic multidecadal oscillation and its relation to  
10 rainfall and river flows in the continental US, *Geophys. Res. Lett.*, 28, 2077–2080,  
11 doi: 10.1029/2000GL012745.

12 Evan, A. (2012), Aerosols and Atlantic aberrations, *Nature*, 484, 170–171.  
13 doi:10.1038/nature11037.

14 Folland, C. K., et al. (1984), Worldwide marine temperature fluctuations 1856–1981,  
15 *Nature*, 310, 670–673, doi:10.1038/310670a0.

16 Ghil, M., and R. Vautard (1991), Interdecadal oscillations and the warming trend in  
17 global temperature time series, *Nature*, 305, 324–327, doi:10.1038/350324a0.

18 Ghil M., et al. (2002), Advanced spectral methods for climatic time series, *Rev. Geophys.*,  
19 40(1), 3.1–3.41, doi:10.1029/2000GR000092.

20 Girs, A. A. (1971), Multiyear oscillations of atmospheric circulation and long-term  
21 meteorological forecasts, *L. Gidrometeroizdat* (in Russian).

22 Hurrell, J. W. (1995), Decadal trends in the North Atlantic Oscillation: Regional  
23 temperatures and precipitation, *Science*, 269, 676–679, doi:

1           10.1126/science.269.5224.676.

2   Kaplan A., et al. (1998), Analyses of global sea surface temperature 1856–1991, *J.*  
3           *Geophys. Res.*, 103, 18,567–18,589, doi:10.1029/97JC01736.

4   Knight, J. R., et al. (2005), A signature of persistent natural thermohaline circulation  
5           cycles in observed climate, *Geophys. Res. Lett.*, 32, L20708, doi:  
6           10.1029/2005GL02423.

7   Kosaka Y. and Xie, S.-P. (2013), Recent global-warming hiatus tied to equatorial Pacific  
8           surface cooling. *Nature*, 501, 403-407, doi:10.1038/nature12534.

9   Kravtsov, S., et al. (2011), On the mechanisms of late 20th century sea-surface  
10           temperature trends over the Antarctic Circumpolar Current, *J. Geophys. Res.*  
11           *Oceans*, 116, 1978–2012, doi: 10.1029/2011JC007473.

12   Kushnir Y., et al. (2002), Atmospheric GCM response to extratropical SST anomalies:  
13           Synthesis and evaluation, *J. Climate*, 15, 2233–2256, doi:  
14           [http://dx.doi.org/10.1175/1520-0442\(2002\)015<2233:AGRTES>2.0.CO;2](http://dx.doi.org/10.1175/1520-0442(2002)015<2233:AGRTES>2.0.CO;2).

15   Mann, M. E., et al. (2014), On forced temperature changes, internal variability, and the  
16           AMO, *Geophys. Res. Lett.*, 41, 3211–3219, doi:10.1002/2014GL059233.

17   Mantua N. J., et al. (1997), A Pacific interdecadal climate oscillation with impacts on  
18           salmon production, *Bull. Am. Meteorol. Soc.*, 78, 1069–1079, doi:  
19           [http://dx.doi.org/10.1175/1520-0477\(1997\)078<1069:APICOW>2.0.CO;2](http://dx.doi.org/10.1175/1520-0477(1997)078<1069:APICOW>2.0.CO;2).

20   Meehl, G. A. et al. (2007), in *IPCC Climate Change 2007: The Physical Science Basis.*  
21           Contribution of Working Group I to the Fourth Assessment Report of the  
22           Intergovernmental Panel on Climate Change, Solomon, S., Ed., Cambridge Univ.

1 Press, pp. 747–845.

2 Minobe, S. (1997), A 50–70-year climatic oscillation over the North Pacific and North  
3 America, *Geophys. Res. Lett.*, 24, 683–686, doi: 10.1029/97GL00504.

4 Minobe, S. (1999), Resonance in bidecadal and pentadecadal climate oscillations over  
5 the North Pacific: Role in climatic regime shifts, *Geophys. Res. Lett.*, 26, 855–  
6 858, doi: 10.1029/1999GL900119.

7 Monahan, A. H., et al. (2009), Empirical Orthogonal Functions: The medium is the  
8 message, *J. Climate*, 22, 6501–6514, doi:  
9 <http://dx.doi.org/10.1175/2009JCLI3062.1>.

10 Moron, V., et al. (1998), Trends, interdecadal and interannual oscillations in global sea-  
11 surface temperatures, *Climate Dyn.*, 14, 545–569, doi: 10.1007/s003820050241.

12 Nagashima, T., et al. (2006), The effect of carbonaceous aerosols on surface temperatures  
13 in the mid 20th century, *Geophys. Res. Lett.*, 33, L04702, doi:  
14 10.1029/2005GL024887.

15 Schlesinger, M. E., and N. Ramankutty (1994), An oscillation in the global climate  
16 system of period 65–70 years, *Nature*, 367, 723–726, doi:10.1038/367723a0.

17 Smith, T. M., et al. (2008), Improvements to NOAA’s historical merged land–ocean  
18 surface temperature analysis (1880–2006), *J. Climate*, 21, 2283–2296, doi:  
19 <http://dx.doi.org/10.1175/2007JCLI2100.1>.

20 Stevens, B. (2013), Aerosols: Uncertain then, irrelevant now, *Nature*, 503, 47–48,  
21 doi:10.1038/503047a.

22 Tsonis, A. A., et al. (2007), A new dynamical mechanism for major climate shifts,

- 1 Geophys. Res. Lett., 34, L13705, doi:10.1029/2007GL030288.
- 2 Vangenheim, G. Ya. (1940), The long-term temperature and ice break-up forecasting,  
3 Proc. State Hydrol. Inst. Iss., 10, 207–236 (in Russian).
- 4 Wyatt, M. G., et al. (2012), Atlantic Multidecadal Oscillation and Northern Hemisphere's  
5 climate variability, *Climate Dyn.*, 38(5–6), 929–949, doi:10.1007/s00382-011-  
6 1071-8.
- 7 Wyatt, M. G., and J. M. Peters (2012), A secularly varying hemispheric climate-signal  
8 propagation previously detected in instrumental and proxy data not detected in  
9 CMIP3 data base, SpringerPlus, 1–68, doi:10.1186/2193-1801-1-68.
- 10 Wyatt, M. G., and J. A. Curry (2014), Role for Eurasian Arctic shelf sea ice in a secularly  
11 varying hemispheric climate signal during the 20th century, *Climate Dyn.*, 42,  
12 2763–2782, doi: 10.1007/s00382-013-1950-2.
- 13

1  
2  
3  
4  
5  
6  
7  
8  
9  
10  
11  
12  
13  
14  
15  
16

**Table captions**

**Table 1:** Climate index definitions and abbreviations. The same indices were used by *Wyatt et al.* [2012] except for the DP index based here on the ERSST data. The acronyms SST and SLP stand for “sea-surface temperature” and “sea-level pressure,” respectively.

**Table 2:** Stadium-wave phase uncertainties for the climate index set defined in Table 1 (see also Fig. 1, left panel). The stadium wave cycle length for this data set is  $68 \pm 4.3$  yr, with the 98% uncertainty range of 64–81 yr. The phase of each index here was defined as the location of the first maximum of its stadium-wave reconstruction. All uncertainties were computed using the Monte-Carlo procedure outlined in text. Comment: *The spread of the phases among different indices (irrespective of the sign) is larger than the phase uncertainty, thus suggesting real stadium-wave propagation in the phase space of climate indices.*

1  
2  
3  
4  
5  
6  
7  
8  
9  
10  
11  
12  
13  
14  
15  
16  
17  
18  
19  
20  
21  
22  
23  
24

## Figure captions

**Figure 1:** The observed stadium wave defined as the sum of two leading M-SSA modes

for the 7-member set of annual climatic indices (see Table 1). Left panel: normalized stadium-wave reconstructions of each index. Right panel: actual (blue) and synthetic (red) time series for the AMO index; light lines show raw time series, while heavy lines — the sum of linear trend and the leading M-SSA pair reconstruction. See text for details on the generation of synthetic time series.

We removed linear trends from each index and normalized each residual time series by its standard deviation prior to applying M-SSA with window size  $M=30$  yr. Comments: (i) *The M-SSA filtered indices share a common timescale, but exhibit a range of phases, which defines the stadium wave “propagation.”* (ii) *The phases of the stadium wave are subject to uncertainty.*

**Figure 2:** The “stadium wave” in the 20<sup>th</sup> century simulations of the GFDL CM3 model;

we looked at the same climate-index subspace as in Fig. 1 except for the AT index, which was not included. Left panel: ensemble-mean of stadium-wave reconstructions for each index over 5 available GFDL simulations. Right panel: the leading principal component (PC) of the M-SSA stadium-wave reconstruction for individual runs (see legend, which also shows the percentage of the reconstructed variance accounted for by this leading PC). We removed linear trends from each index and normalized each residual time series by its standard deviation prior to applying M-SSA with window size  $M=30$  yr. Comments: (i) *The M-SSA filtered indices share a common in-phase signal for all runs,*

1        *suggesting it to represent a forced climate response. (ii) The phases of this forced*  
2        *signal vary slightly from simulation to simulation, reflecting uncertainties of our*  
3        *identification procedure.*

4        **Figure 3:** Regression (map units: °C) of the observed (ERSST: left) and simulated  
5        (ensemble average of the five GFDL’s 20<sup>th</sup> century runs: right) SST time series  
6        (1900–1999) onto linear trend (top), as well as onto 75-yr-periodic sine (middle)  
7        and cosine (bottom) predictors; zero phase for these harmonic predictors was  
8        chosen to correspond to year 1920. All three predictors were normalized to unit  
9        variance, with the resulting ranges over the 20<sup>th</sup> century of 3.4 units for the trend  
10       and 2.9 units for the sine and cosine predictors. We smoothed each SST time  
11       series by the 20-yr boxcar running-mean filter prior to computing regressions.

12       Comment: *Multidecadal climate variability in GFDL CM3 is characterized by a*  
13       *reasonable trend, underestimated sine pattern in the Atlantic and essentially non-*  
14       *existent cosine pattern.*

15       **Figure 4:** Spectra of the observed and GFDL simulated climate indices. The spectra are  
16       defined here as the variance of the boxcar-running-mean averaged time series for  
17       different window sizes. The abscissa on all plots shows half the window size in  
18       units of years, with 0 corresponding to no averaging (raw annual data), 1 — to 3-  
19       yr boxcar averages, 2 — to 5-yr boxcar averages and so on. The blue line shows  
20       the observed spectra based on the ERSST/20<sup>th</sup>-century reanalysis indices, and the  
21       red dashed lines show the range of spectral estimates over those for 5 individual  
22       20<sup>th</sup> century runs. Index names are listed in the caption of each panel. Comments:  
23       (i) *The GFDL CM3 model matches well the observed variance of raw (unfiltered)*

1        *data for all indices, and that throughout the whole spectral range for the NHT*  
2        *and PDO indices. (ii) However, the GFDL-based variance of low-frequency*  
3        *(multidecadal) behavior for other indices (DP, AMO, NAO, and ALPI) is smaller*  
4        *than the observed variance by a factor of 5–10.*

1

2 **Table 1:** Climate index definitions and abbreviations \*

Index/Acronym	Reference/source	Description
<b>Atlantic Dipole/DP</b>	ERSST data set <i>Smith et al.</i> [2008]	Difference in SST area averages between the (60°–10°W, 40°–60°N) and (50°–0°W, 60°–40°S)
<b>NH surface temperature/NHT</b>	HadCRUT3 data set <i>Brohan et al.</i> [2006]	Average land-surface temperatures and SSTs of Northern Hemisphere
<b>Atlantic Multidecadal Oscillation/AMO</b>	<i>Kaplan et al.</i> [1998] SST data set	North Atlantic SST averaged across 0–60°N, 75–7.5°W
<b>Atmospheric Mass Transfer/AT</b>	[ <i>Vangenheim</i> , 1940; <i>Girs</i> , 1971]	Prevailing air transfer direction 30°–80°N; 45–75°E
<b>North Atlantic Oscillation/NAO</b>	<i>Hurrell</i> [1995]	Normalized SLP difference between Azores and Iceland, wintertime values (DJFM) were used
<b>Pacific Decadal Oscillation/PDO</b>	[ <i>Mantua et al.</i> , 1997; <i>Minobe</i> , 1997, 1999]	Leading principal component of monthly SST north of 20°N in the North Pacific, with century-scale globally averaged SST signal removed
<b>Aleutian Low Pressure/ALPI</b>	<i>Beamish et al.</i> [1997]	Mean area of the North Pacific region with monthly SLP < 1005 mb during winter (DJFM)

3

4 \*The same indices were used by *Wyatt et al.* [2012] except for the DP index based here  
5 on the ERSST data. The acronyms SST and SLP stand for “sea-surface temperature” and  
6 “sea-level pressure,” respectively.

7

1

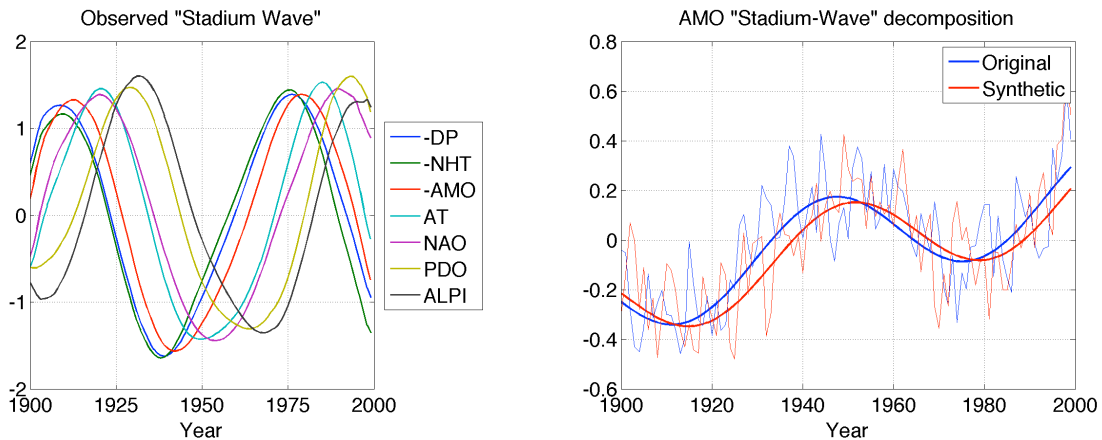
2 **Table 2:** Stadium-wave phase uncertainties for the climate index set defined in Table 1\*

<b>Index name</b>	<b>-DP</b>	<b>-NHT</b>	<b>-AMO</b>	<b>AT</b>	<b>NAO</b>	<b>PDO</b>	<b>ALPI</b>
<b>Phase/STD</b>	1908±2.9	1907±3	1912±2.7	1919±3.2	1921±6.5	1929±3.3	1932±5
<b>Phase 90% range</b>	1903 – 1913	1901 – 1911	1907 – 1915	1914 – 1924	1911 – 1932	1924 – 1934	1924 – 1940

3

4 \*(See also Fig. 1, left panel.) The stadium wave cycle length for this data set is  $68 \pm 4.3$  yr,  
5 with the 98% uncertainty range of 64–81 yr. The phase of each index here was defined as  
6 the location of the first maximum of its stadium-wave reconstruction. All uncertainties  
7 were computed using the Monte-Carlo procedure outlined in text. *Comment: The spread*  
8 *of the phases among different indices (irrespective of the sign) is larger than the phase*  
9 *uncertainty, thus suggesting real stadium-wave propagation in the phase space of climate*  
10 *indices.*

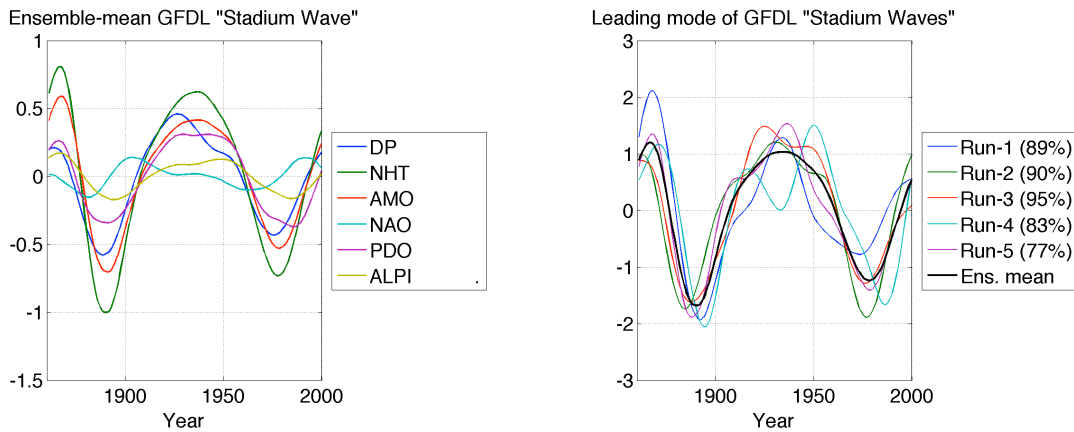
1



2 **Figure 1:** The observed stadium wave defined as the sum of two leading M-SSA modes  
3 for the 7-member set of annual climatic indices (see Table 1). Left panel:  
4 normalized stadium-wave reconstructions of each index. Right panel: actual  
5 (blue) and synthetic (red) time series for the AMO index; light lines show raw  
6 time series, while heavy lines — the sum of linear trend and the leading M-SSA  
7 pair reconstruction. See text for details on the generation of synthetic time series.  
8 We removed linear trends from each index and normalized each residual time  
9 series by its standard deviation prior to applying M-SSA with window size  $M=30$   
10 yr. Comments: (i) *The M-SSA filtered indices share a common timescale, but*  
11 *exhibit a range of phases, which defines the stadium wave “propagation.”* (ii) *The*  
12 *phases of the stadium wave are subject to uncertainty.*

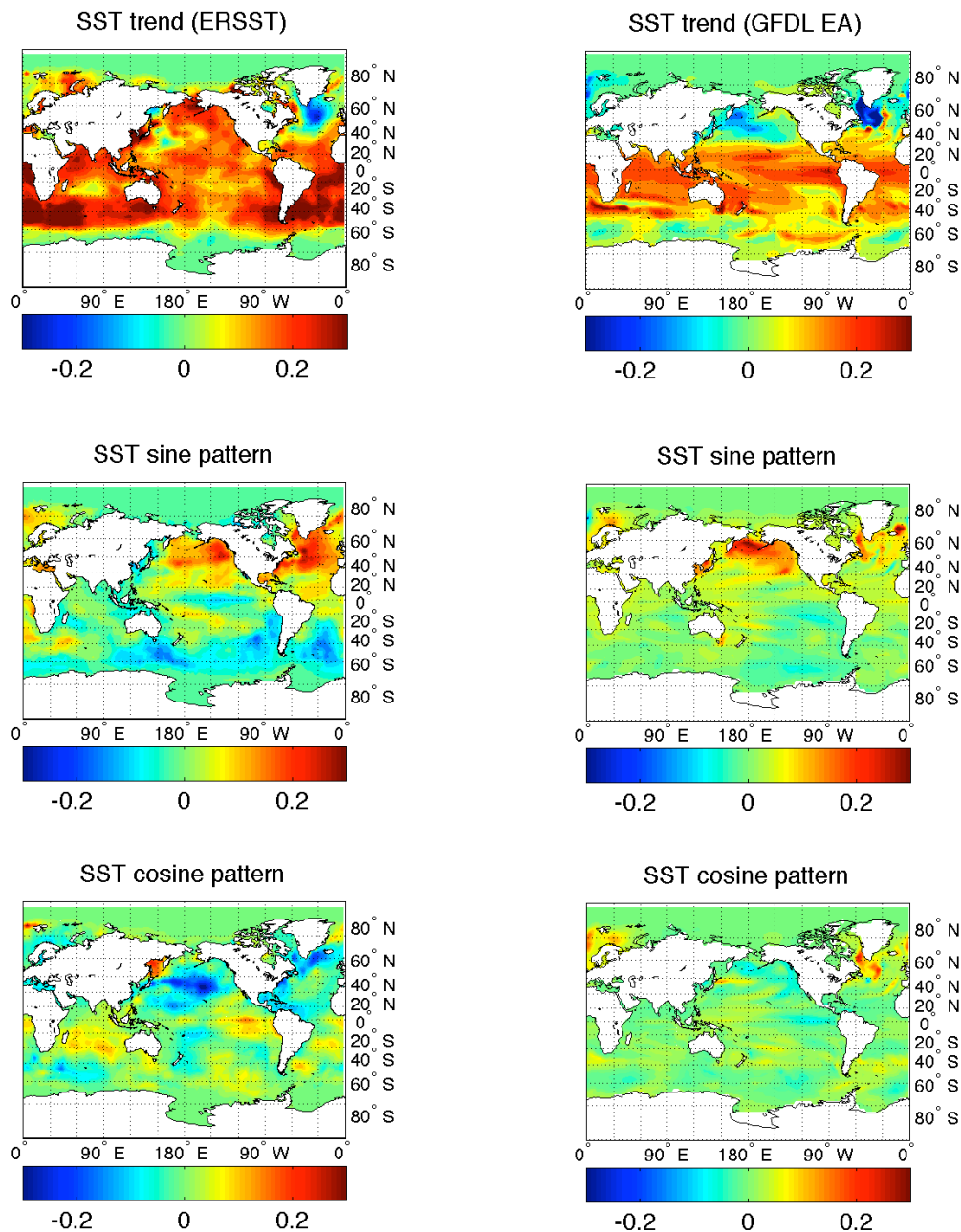
13

1

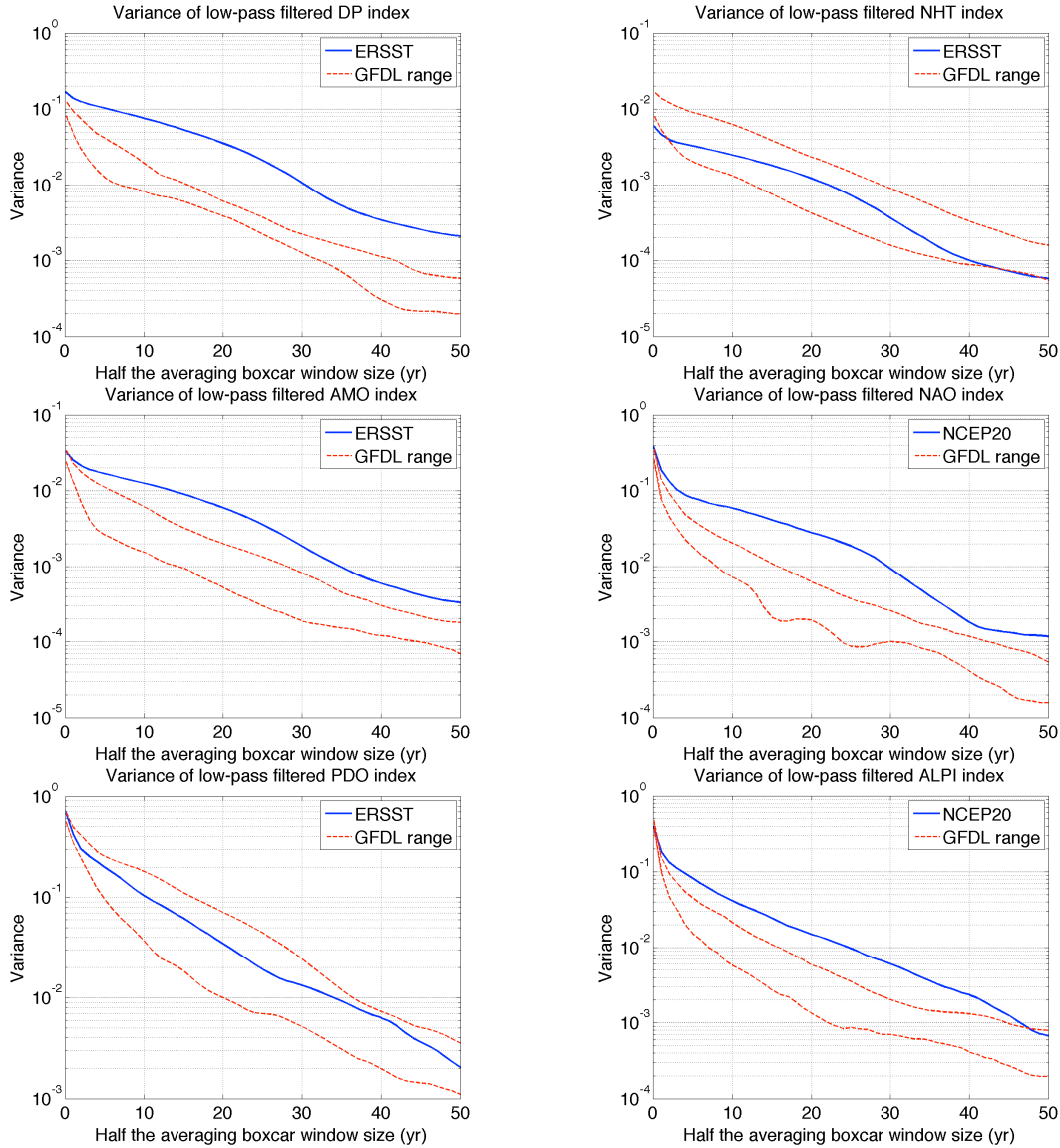


2 **Figure 2:** The “stadium wave” in the 20<sup>th</sup> century simulations of the GFDL CM3 model;  
3 we looked at the same climate-index subspace as in Fig. 1 except for the AT index,  
4 which was not included. Left panel: ensemble-mean of stadium-wave  
5 reconstructions for each index over 5 available GFDL simulations. Right panel:  
6 the leading principal component (PC) of the M-SSA stadium-wave reconstruction  
7 for individual runs (see legend, which also shows the percentage of the  
8 reconstructed variance accounted for by this leading PC). We removed linear  
9 trends from each index and normalized each residual time series by its standard  
10 deviation prior to applying M-SSA with window size  $M=30$  yr. Comments: (i)  
11 *The M-SSA filtered indices share a common in-phase signal for all runs,*  
12 *suggesting it to represent a forced climate response.* (ii) *The phases of this forced*  
13 *signal vary slightly from simulation to simulation, reflecting uncertainties of our*  
14 *identification procedure.*

15



1 **Figure 3:** Regression (map units: °C) of the observed (ERSST: left) and simulated  
2 (ensemble average of the five GFDL's 20<sup>th</sup> century runs: right) SST time series  
3 (1900–1999) onto linear trend (top), as well as onto 75-yr-periodic sine (middle)  
4 and cosine (bottom) predictors; zero phase for these harmonic predictors was  
5 chosen to correspond to year 1920. All three predictors were normalized to unit  
6 variance, with the resulting ranges over the 20<sup>th</sup> century of 3.4 units for the trend  
7 and 2.9 units for the sine and cosine predictors. We smoothed each SST time  
8 series by the 20-yr boxcar running-mean filter prior to computing regressions.  
9 *Comment:* Multidecadal climate variability in GFDL CM3 is characterized by a  
10 reasonable trend, underestimated sine pattern in the Atlantic and essentially non-  
11 existent cosine pattern.



1

2 **Figure 4:** Spectra of the observed and GFDL simulated climate indices. The spectra are  
3 defined here as the variance of the boxcar-running-mean averaged time series for  
4 different window sizes. The abscissa on all plots shows half the window size in  
5 units of years, with 0 corresponding to no averaging (raw annual data), 1 — to 3-  
6 yr boxcar averages, 2 — to 5-yr boxcar averages and so on. The blue line shows  
7 the observed spectra based on the ERSST/20<sup>th</sup>-century reanalysis indices, and the  
8 red dashed lines show the range of spectral estimates over those for 5 individual  
9 20<sup>th</sup> century runs. Index names are listed in the caption of each panel. *Comments:*  
10 (i) *The GFDL CM3 model matches well the observed variance of raw (unfiltered)*  
11 *data for all indices, and that throughout the whole spectral range for the NHT*  
12 *and PDO indices. (ii) However, the GFDL-based variance of low-frequency*  
13 *(multidecadal) behavior for other indices (DP, AMO, NAO, and ALPI) is smaller*  
14 *than the observed variance by a factor of 5–10.*